Characterization of the Solar H-alpha Spectrum Using Lunt 50 mm Telescope with Pressure Tuning

G. Bergamin, A. Bemporad, C. Benna

Introduction

In this work we present the study of the Lunt LS50 Hα telescope equipped with a CMOS QHY5LII-C camera and the capability of reconstructing the solar spectrum through full-disk images of the Sun at different pressure tuning steps of the telescope. Furthermore, specific solar regions and structures were analyzed to obtain a profile comparable to the expected Hα spectrum. This allows us to investigate important physical parameters, such as temperature and height of the studied structures.

1 Introduction

The Sun can be studied at different wavelengths. Among them, the Hα line is the most accessible with amateur-level telescopes. The spectral line of neutral hydrogen corresponds to a wavelength $\lambda = 656.28$ nm, and it is an emission/absorption line produced by neutral hydrogen (H I). This transition belongs to the Balmer series, corresponding to the electronic transition from $n = 3$ to $n = 2$.

Studying this spectral line is of great importance since it allows us to observe the solar chromosphere, i.e. the region above the photosphere where dynamic phenomena such as prominences, spicules, flares, and bright plages originate.

In this work, a particular type of instrument is employed (see Section 2): a solar telescope specifically designed to isolate this spectral line of neutral hydrogen.

2 Instrumentation and Calibration

2.1 Optical Instrumentation: the Lunt LS50 Hα Telescope

The telescope used for this work is a Lunt Solar Systems LS50 Hα telescope, with a 50 mm aperture and 300 mm focal length (Figure 1). This telescope is equipped with an upgraded system allowing band shifting through a *Pressure Tuning* mechanism, applied directly to the internal etalon.

Figure 1: The Lunt LS50 Hα telescope used in this study.

2.2 Etalons and Their Operation

In solar instrumentation, the key element for selecting a narrow spectral region is the *etalon* (Fabry-Perot interferometer). The etalon generally consists of two parallel plates with partially reflective surfaces. Incoming light is multiply reflected inside the cavity, and due to interference effects, only specific wavelengths are transmitted constructively, while others are suppressed.

Different manufacturing techniques exist for building etalons. Broadly, they can be categorized as:

- **Mechanical (air-spaced) etalons**, where the two plates are separated by a thin air gap. The transmitted wavelength can be tuned either by varying the spacing of the plates or by changing the internal pressure, which modifies the refractive index of the medium inside.
- **Electronic (solid-state) etalons**, where the cavity material is electro-optically active and the transmitted wavelength is controlled by applying an external voltage.

In this study, we use an **air-spaced etalon with pressure tuning**. This system, also known as "True Doppler Tuning," works by slightly changing the internal air pressure, shifting the transmission wavelength toward the red or blue side of the Hα line. By scanning through different pressure values, it becomes possible to probe different atmospheric layers of the solar chromosphere.

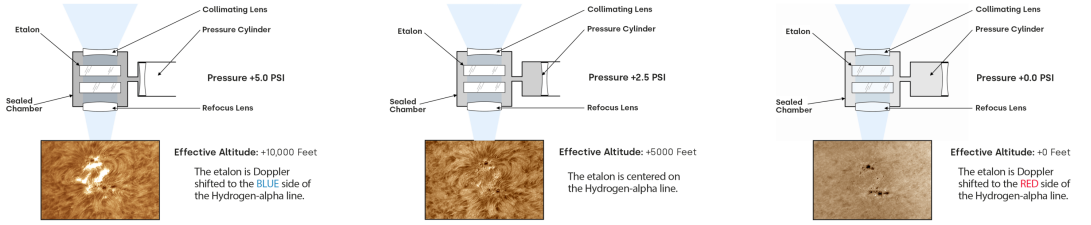

2.3 Blocking Filter

The blocking filter (BF) is a fundamental element of solar telescopes operating in the Hα line. Its main function is to ensure that only the extremely narrow spectral region around 656.28 nm reaches the camera, while suppressing all unwanted wavelengths.

The filter is not a single optical element, but a combination of multiple dielectric and absorption filters stacked together. This layered structure achieves two important goals:

- **Spectral selectivity:** the BF removes residual sidebands and multiple transmission peaks that arise naturally from the etalon's periodic transmission function. Without it, several spurious orders of the Fabry-Perot would be visible, resulting in an image contaminated by broadband photospheric light.
- **Observer safety:** the filter attenuates the intense solar flux outside the Hα line, preventing excessive radiation (especially infrared and ultraviolet) from reaching the eye or the detector. This is crucial to avoid both damage to the camera sensor and potential danger for visual observations.

In practice, the BF used in the Lunt LS50 telescope has a passband of approximately 6–10 Å centered on Hα, sufficiently broad to fully transmit the narrow core defined by the etalon but narrow enough to eliminate out-of-band leakage. The combined action of the etalon and blocking filter results in a system that isolates only the desired solar chromospheric features with high contrast.

Figure 2: The Lunt LS50 Hα BF.

2.4 Imaging Camera

The imaging device plays a crucial role in determining the spatial and temporal resolution of the data. For this study we employed a **QHY5LII-C planetary camera**, which is a compact CMOS-based detector optimized for high-frame-rate astrophotography.

The sensor used in this camera is the Micron MT9M034, with the following key specifications:

- **Resolution:** 1280 × 960 pixels (1.2 Megapixel).
- **Pixel size:** 3.75 µm, providing a good compromise between sensitivity and resolution.
- **Sensor type:** CMOS, which allows for low readout noise and rapid frame acquisition compared to traditional CCD sensors.
- **Quantum efficiency:** optimized in the visible range, with a significant peak around the Hα wavelength (656 nm).

One of the advantages of this camera is its capability to operate at high frame rates (up to tens of frames per second), which is extremely beneficial in solar observations. The atmospheric turbulence ("seeing") constantly distorts the incoming wavefront, but by recording a large number of frames, it becomes possible to later select and average the sharpest ones (a technique known as *lucky imaging*).

Additionally, the relatively small pixel size ensures a proper sampling of the solar image produced by the telescope's 300 mm focal length. When combined with suitable region-of-interest (ROI) selection, the QHY5LII-C provides flexibility: it can be used both for full-disk imaging and for detailed studies of active regions such as sunspots and prominences.

This versatility, together with its low cost and compact size, makes the planetary CMOS camera a valuable tool for semi-professional solar spectroscopy and imaging.

2.5 Camera Parameter Calibration

To ensure a linear response and optimal dynamic range for spectral reconstruction, a preliminary calibration of the camera's acquisition parameters was performed. The quality of the final image, and therefore the accuracy of the extracted Hα profile, strongly depends on three main variables: exposure time, sensor gain, and the total number of frames acquired.

- **Exposure Time:** In solar imaging, exposure times must be kept as short as possible (typically in the order of a few milliseconds) to "freeze" the atmospheric seeing. However, the exposure must remain long enough to adequately sample the signal, especially when tuning the etalon into the darker wings of the Hα line.
- **Gain:** Increasing the analog gain amplifies the signal but simultaneously reduces the sensor's dynamic range and increases the overall noise floor. For quantitative spectroscopic analysis, the gain must be carefully optimized to preserve linearity and strictly avoid pixel saturation (clipping) in high-intensity regions, such as plages.
- **Number of Frames:** The *lucky imaging* technique relies on recording a large video sequence containing N frames. By assessing the sharpness of each frame, we select and stack only the best percentage. Statistically, stacking multiple frames significantly improves the Signal-to-Noise Ratio (SNR), which scales proportionally to the square root of the stacked frames (SNR $\propto \sqrt{N_{\text{stacked}}}$).

To determine the optimal configuration, multiple acquisition sets were recorded with varying combinations of gain and exposure. The pixel intensity distributions were then evaluated using image histograms. Analyzing the histograms allows us to verify that the signal occupies the widest possible dynamic range without saturating the sensor (which would appear as a spike at the maximum pixel value on the right edge of the histogram).

To determine the optimal configuration thanks to the histograms, the intensity of the central pixel was plotted against varying values of exposure, gain, and number of frames (Figure 3).

Analyzing these relationships is crucial to avoid pixel saturation, which occurs when the intensity reaches the sensor's digital limit (producing a flat plateau at approximately 65,000 counts in the graphs). Based on the plotted curves, we deduced the optimal combination of parameters to maximize the signal while remaining in the linear regime:

- **Exposure Time:** The intensity increases linearly until it reaches a saturation plateau at an exposure value of 2.5. Consequently, a value of **2.0** was chosen to maintain a high signal-to-noise ratio while avoiding clipping in the brightest solar regions.
- **Gain:** The sensor response shows a steep increase followed by a saturation plateau starting at a gain of 10. To preserve linearity and dynamic range, a gain of **8** was selected for the final acquisitions.
- **Number of Frames:** The intensity of the central pixel peaks at **200 frames**. Beyond this point, the intensity slightly decreases; this suggests that adding more frames introduces lower-quality data affected by atmospheric seeing, which tends to blur the sharpest features and reduce the peak intensity of the stacked result.

This optimized combination (Exposure = 2.0, Gain = 8, Frames = 200) ensures that the sensor's dynamic range is fully utilized without loss of information due to overexposure.

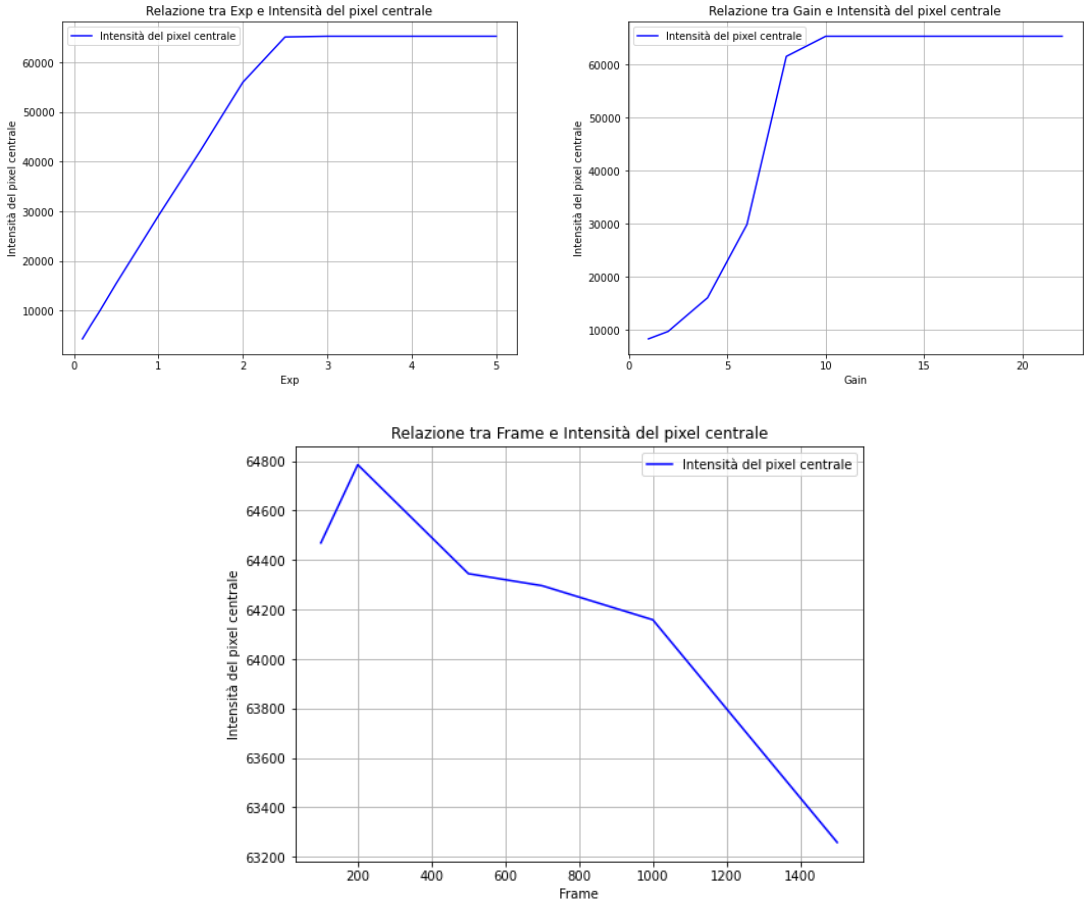

Figure 3: Calibration curves showing the relationship between central pixel intensity and Exposure (top left), Gain (top right), and Number of Frames (bottom).

3 Theoretical Background

Before analyzing the acquired images, it is useful to outline the theoretical model describing the solar Hα absorption profile.

The intrinsic solar line profile can be approximated by a Gaussian function:

$$G(x) = \frac{1}{\sigma\sqrt{2\pi}} \exp\left(-\frac{x^2}{2\sigma^2}\right), \tag{1}$$

where σ is the standard deviation. Its full width at half maximum (FWHM) is:

$$\mathrm{FWHM}_G = 2\sqrt{2\ln 2}\,\sigma. \tag{2}$$

The transmission profile of the etalon is well described by a Lorentzian function:

$$L(x) = \frac{\gamma}{\pi\left(\gamma^2 + x^2\right)}, \tag{3}$$

with FWHM:

$$\mathrm{FWHM}_L = 2\gamma. \tag{4}$$

The observed profile is given by the convolution of the Gaussian and Lorentzian functions, resulting in a Voigt profile. Its effective width is:

$$\mathrm{FWHM}_V = \frac{\mathrm{FWHM}_L}{2} + \sqrt{\left(\frac{\mathrm{FWHM}_L}{2}\right)^2 + \mathrm{FWHM}_G^2}. \tag{5}$$

4 Data Acquisition and Analysis

Images of the full solar disk and selected regions of interest (sunspots, plages, filaments, and prominences) were obtained systematically across several pressure tuning steps of the Fabry-Pérot etalon. By extracting and measuring the intensity variations of specific pixels or regions across this image sequence, we successfully reconstructed the solar Hα absorption line profile.

The reference profile provided by NASA yields a Gaussian Full Width at Half Maximum of $\mathrm{FWHM}_G = 1.3269$ Å for the solar Hα line. The telescope's etalon has a Lorentzian profile with $\mathrm{FWHM}_L = 0.7$ Å. The convolution of these thermal, turbulent, and instrumental broadening effects results in an observed profile accurately described by a Voigt function. Fitting this Voigt function to our empirical data allows for a precise wavelength calibration of the etalon's pressure tuning mechanism. For this specific instrumental setup, we estimate the tuning increment to be:

$$\Delta\lambda \approx 0.21 \text{ Åper image step}$$

This calibration is critical, as it translates arbitrary pressure steps into a physical wavelength scale, enabling a direct and quantitative comparison between theoretical atmospheric models and the reconstructed spectral profiles from our acquired data.

5 Results on Solar Regions

5.1 Surface (Quiet Sun)

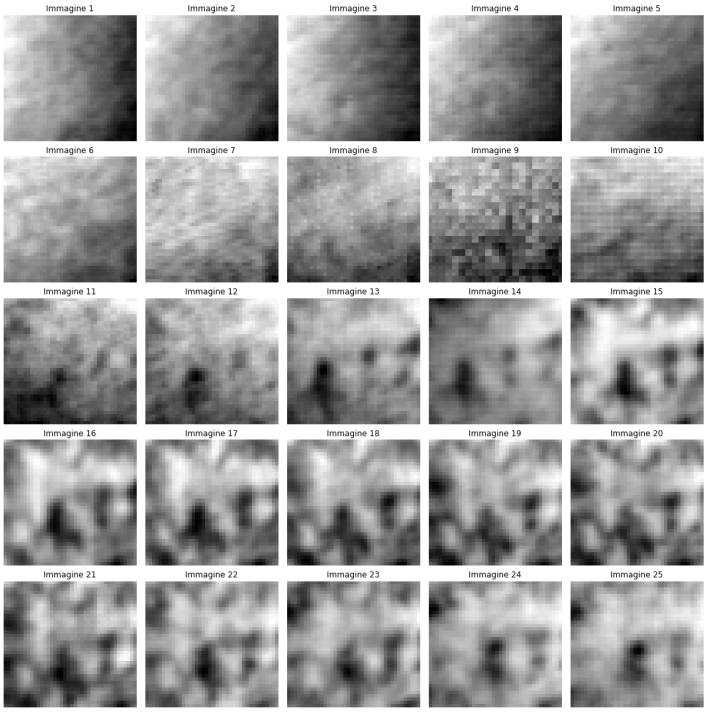

Figure 4: Example of a surface Hα image of the Sun at a specific pressure tuning step.

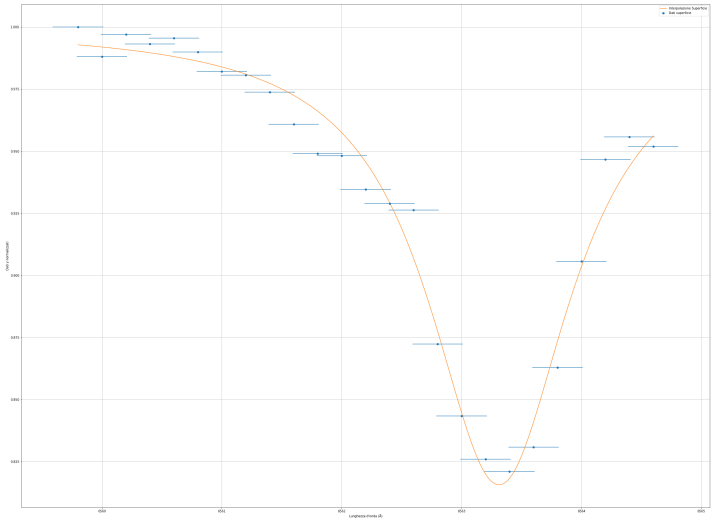

Figure 5: Normalized brightness profile obtained from surface measurements, representing the baseline Quiet Sun absorption.

Analysis: The surface Hα profile serves as our experimental baseline. In this dataset, the Quiet Sun (represented by the red points and grey interpolation) exhibits the **deepest absorption core** among all observed regions, reaching a minimum normalized intensity of approximately 0.82. The $H\alpha$ transition at 6562.8 Å is a strong Fraunhofer line originating in the solar chromosphere; its depth here indicates a region of standard thermal absorption undisturbed by significant magnetic heating or localized emission. This profile is the most sensitive to the average chromospheric temperature gradient, providing the necessary reference to quantify the "core filling" observed in active regions.

5.2 Plage Regions

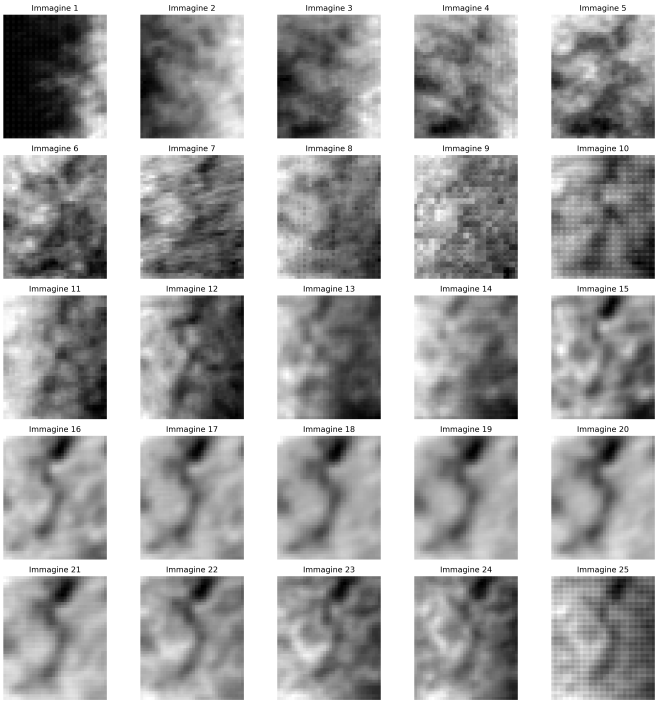

Figure 6: Selected plage regions imaged at multiple tuning steps, appearing as bright patches in the chromosphere.

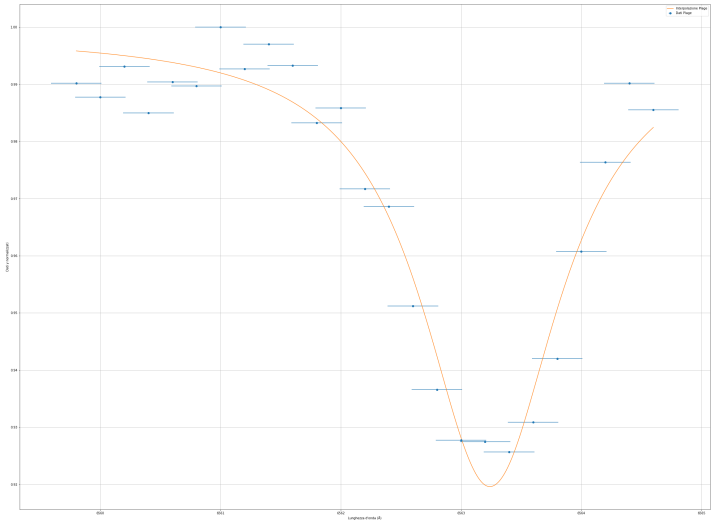

Figure 7: Intensity profile of plage regions across the Hα line, exhibiting noticeable core filling.

Analysis: Plages are bright, magnetically active regions where magnetic energy dissipation heats the local plasma. Our data (orange points and brown interpolation) clearly shows the **core filling** effect: the minimum intensity reaches approximately 0.93, which is significantly higher than the quiet surface. This occurs because the increased temperature and electron density in the plage chromosphere enhance collisional excitation, leading to localized emission within the $H\alpha$ line. This emission partially offsets the absorption, resulting in a shallower profile and a higher central intensity compared to the baseline.

5.3 Filaments

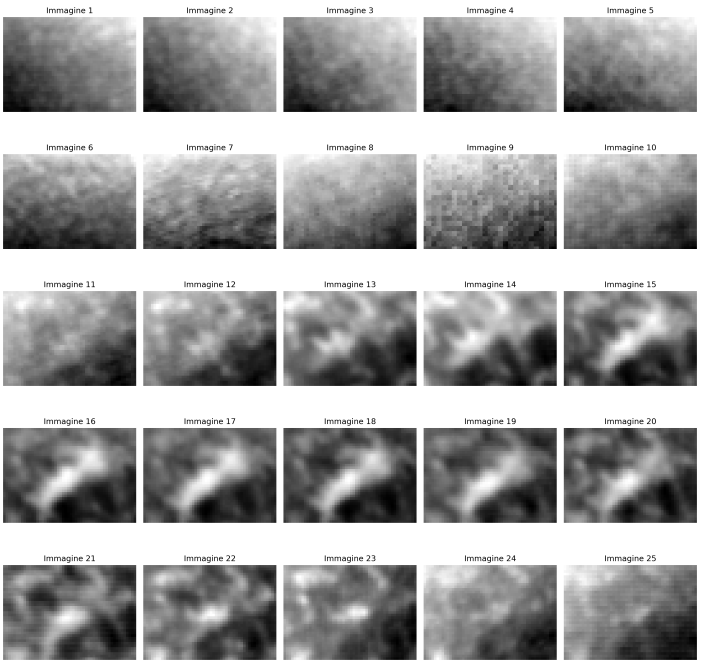

Figure 8: Filament structures observed as dark ribbons in Hα against the solar disk.

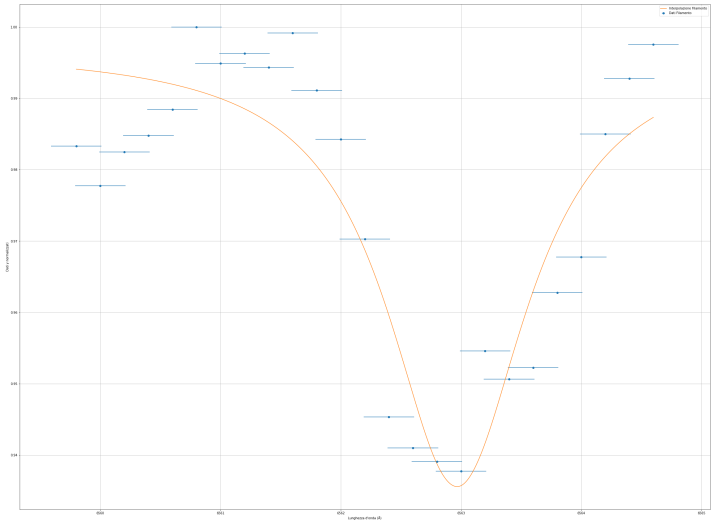

Figure 9: Spectral profile of filaments across the Hα line, showing enhanced absorption.

Analysis: Filaments are typically described as dense, cool clouds of plasma. However, in this specific observation (green points and pink interpolation), the filament exhibits the **highest core intensity** in the entire spectrum (≈ 0.94), appearing even shallower than the plage regions. This suggests that for this particular structure, the contrast relative to the quiet sun

is very low, or that we are observing a "filling" effect where the background chromospheric emission is less obstructed than expected. The proximity of the core intensity to the continuum level indicates a low optical thickness or a high source function in the line-forming layers of this specific filament.

5.4 Sunspots

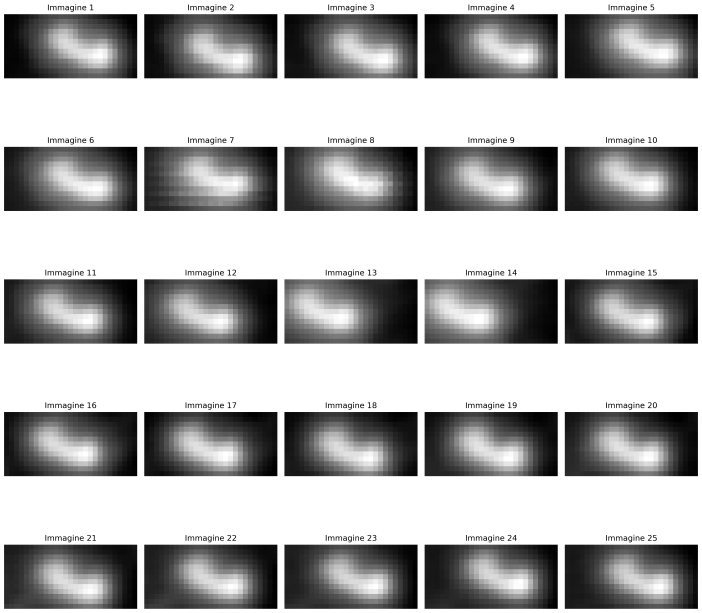

Figure 10: Sunspot observed at different tuning steps, showing the dark umbra and surrounding penumbra.

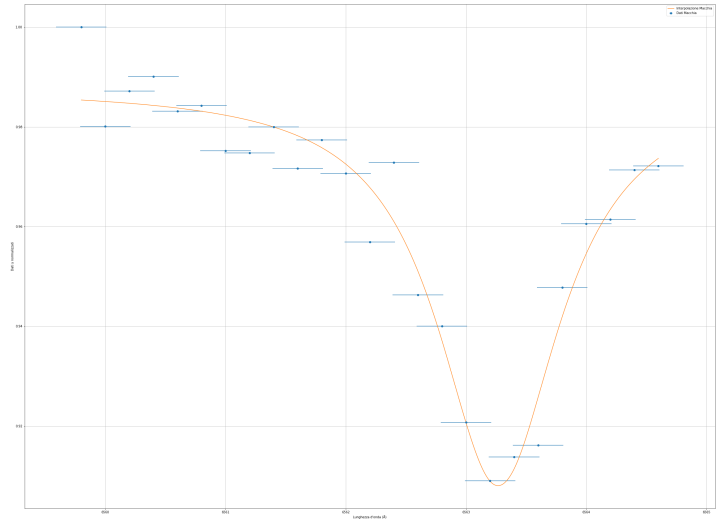

Figure 11: Normalized brightness profile of the sunspot region, demonstrating a significant drop in continuum intensity.

Analysis: Sunspots are characterized by intense magnetic fields that inhibit convection, making them cooler than the surrounding photosphere. While they appear dark in continuum

images, the **normalized** spectral profile (blue points and purple interpolation) shows a core depth of approximately 0.91. This is shallower than the quiet surface (0.82) but deeper than the bright plages. This intermediate depth suggests that while the sunspot environment is cooler, the vertical temperature gradient in its own chromosphere results in a less pronounced absorption dip when compared to the normalized baseline of the Quiet Sun.

5.5 Comparison of All Profiles

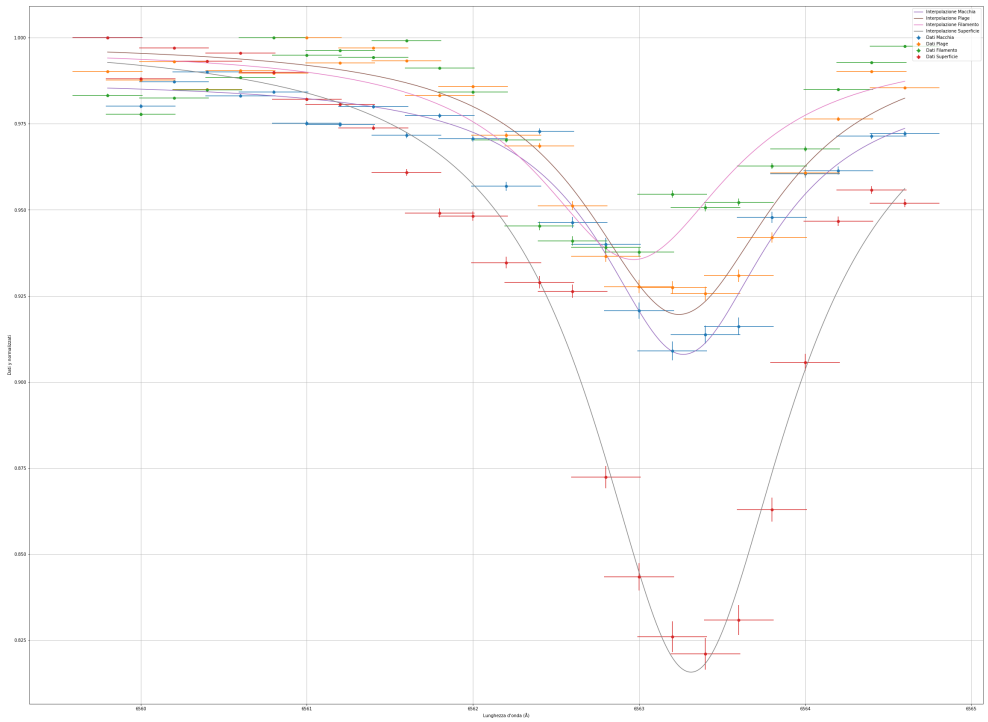

Figure 12: Comparison of normalized Hα profiles. The plot shows the experimental data points with horizontal error bars (wavelength uncertainty) and the corresponding Voigt/Gaussian interpolations.

Analysis: The comparison of the reconstructed profiles (Figure 12) allows for a quantitative diagnostic of the different solar environments. By observing the minimum intensity (core depth) of the normalized profiles, we can draw the following conclusions based on the experimental data:

- **Surface (Quiet Sun):** Represented by the red points and grey interpolation, it exhibits the **deepest absorption core** ($I_{min} \approx 0.82$). This confirms that in the absence of strong magnetic activity, the Hα absorption is most efficient, providing the reference baseline for the solar chromosphere.
- **Sunspots (Macchia):** The blue profile shows a shallower core ($I_{min} \approx 0.91$) compared to the surface. While sunspots are significantly darker in absolute terms, their normalized spectral profile suggests a different temperature gradient in the line-forming layers, resulting in a less pronounced absorption dip.
- **Plage Regions:** The orange profile shows clear evidence of **core filling** ($I_{min} \approx 0.93$). The magnetic heating in the chromosphere above plages increases the source function,

leading to localized emission that partially offsets the absorption, thus raising the core intensity.

- **Filaments:** Interestingly, the filament data (green points, pink line) shows the **highest core intensity** ($I_{min} \approx 0.94$) in this dataset. This indicates a very low contrast relative to the local continuum for this specific feature, suggesting it might be a low-density filament or a region where chromospheric background emission is dominant.

The convergence of all profiles towards unity at ± 2 Å from the center confirms the consistency of the normalization and the reliability of the pressure-tuning calibration ($\Delta\lambda \approx 0.21$ Å/step).

By mapping these spectral variations, the etalon tuning method proves highly effective not just for morphological imaging, but as a robust diagnostic tool for spatially resolved solar spectroscopy.